105 (2026) 108096

Contents lists available at ScienceDirect

Poultry Science

journal homepage: www.elsevier.com/locate/psj

Full-Length Article

Chicoric acid alleviates LPS-induced hepatic inflammation in broilers by regulating the TLR4/MAPK signaling pathway

Qingqing Han [#], Leying Ma [#], Zhanfan He, Shuai Zhou, Gengnan Wang [*]

College of Veterinary Medicine, Hebei Agricultural University, Baoding, Hebei, 071000, China

ARTICLE INFO

Keywords:
Chicoric acid
Hepatic inflammation
MAPK
Lipopolysaccharide

ABSTRACT

Chicoric acid (**CA**) is a natural phenolic acid with well-documented anti-inflammatory properties. This study systematically evaluated the protective effects and underlying mechanisms of CA against lipopolysaccharide (LPS)-induced hepatic inflammation in broilers. Network pharmacology analysis identified 277 overlapping genes associated with hepatic inflammation, and functional enrichment revealed significant involvement of the Toll-like receptor 4 (**TLR4**)/mitogen-activated protein kinase (**MAPK**) signaling pathway. Molecular docking suggested potential stable interactions between CA and core targets, including TLR4, transforming growth factor-β-activated kinase 1 (**TAK1**), c-Jun N-terminal kinase (**JNK**), and p38 MAPK. In vivo, CA markedly ameliorated LPS-triggered hepatic histopathological injury and reduced the secretion of pro-inflammatory cytokines, namely tumor necrosis factor-α (TNF-α), interleukin-1β (**IL-1β**), and interleukin-6 (**IL-6**). In vivo qRT-PCR showed that CA significantly downregulated the mRNA expression of TLR4, TAK1, JNK, and p38 in broiler liver tissues, with a particularly pronounced inhibitory effect on JNK at the transcript level. In LMH cell in vitro assays, qRT-PCR demonstrated that CA reduced the mRNA levels of these targets in LMH cells; cell-based Western blot revealed decreased total TLR4 protein abundance, whereas total TAK1 and p38 protein levels remained unaltered, accompanied by reduced phosphorylation of TAK1 and p38. Collectively, these findings provide correlative pharmacological evidence supporting the development of CA as a natural, antibiotic-alternative hepatoprotective agent for poultry health.

Introduction

Animal-derived foods serve as a critical source of energy, protein, and essential micronutrients for human consumption. Poultry production features a short production cycle, high feed efficiency, and few cultural or religious dietary restrictions, rendering poultry meat and eggs core components of global animal-derived food consumption (Wu et al., 2022). However, the intensification of modern poultry production, while improving production efficiency, has concurrently increased the exposure of broilers to pathogens and various stressors, thereby elevating the risk of inflammatory diseases and oxidative stress injury (Huang et al., 2025; Korver, 2023). Against this background, hepatic inflammation triggered by bacterial infections and other etiological factors has emerged as a major constraint limiting health status and production performance in poultry (Xing et al., 2025).

In intensive rearing environments, Gram-negative bacterial infection and the associated release of endotoxins represent important etiological factors contributing to hepatic inflammation in poultry, with lipopolysaccharide (**LPS**), as the core pathogenic component of endotoxin, warranting particular attention. LPS is a major constituent of the outer membrane of Gram-negative bacteria and a primary inducer of inflammatory responses (Wan et al., 2024). It activates the immune system through signaling pathways involving Toll-like receptor 4 (**TLR4**), nuclear factor-κB (**NF-κB**), and mitogen-activated protein kinases (**MAPK**), promoting excessive accumulation of pro-inflammatory mediators, triggering cytokine storm and oxidative stress, and ultimately leading to hepatic inflammation (Yu et al., 2024). This pathological mechanism is highly conserved across multiple animal species, including humans (Li et al., 2020; Wang et al., 2018). Broilers grow rapidly with vigorous hepatic metabolic activity, imposing substantial physiological burden on the liver and rendering broilers more susceptible to LPS-mediated hepatic injury under commercial rearing conditions (Chen et al., 2024; Mei et al., 2020).This susceptibility predisposes broilers to varying degrees of hepatic inflammation, ranging from subclinical manifestations

* Corresponding author at: No. 2596, Lekai South Street, Baoding, 071000, Hebei, China.
E-mail address: wanggengnan@hebau.edu.cn (G. Wang).
# These authors contributed equally to this study.

https://doi.org/10.1016/j.psj.2026.108096
Received 18 June 2026; Accepted 5 November 2026
Available online 6 November 2026
0032-5791/© 2026 The Authors. Published by Elsevier Inc. on behalf of Poultry Science Association Inc. This is an open access article under the CC BY license (http://creativecommons.org/licenses/by/4.0/).

Table 1
Real-time quantitative PCR primer sequences.

Target	Sequence (5′→3′)	NCBI References
JNK2	F: TCTGGTCTGTTGGGTGCATTTTGG R: GCTGAGGGCGTTCCTAGTTGTTC	XM_046926860.1
JNK1	F: TGAGCAGAAGCAAGCGTGACAAC R: CGCTCAAGGATGGCATCATAGGC	XM_040675395.2
p38	F: CAGATGACGAACCAGTGGCAGAC R: CGGTGGCACAAAGCTGATTACTTC	XM_040691291.2
MYD88	F: AAGGTGTCGGAGGATGGTGGTC R: GGAATCAGCCGCTTGAGACGAG	XM_046910878.1
TAK1	F: CTGGATGGAGTGACTGGCTTCTTG R: TGGCAAACTCTGTGGCTATCATGG	NM_001006240.3
β-actin	F: GCCCTGGCACCTAGCACAATG R: CTCCTGCTTGCTGATCCACATCTG	NM_205518.2
TLR4	F: CGGCTCCGCATCTTGGATAT R: GGGCTTGGAGTGGCTTGTAT	NM_001030693.2
JUN	F: TCAACTCCGCACCCAACTAC R: TCAATAGGGGACAGGGGAGG	NM_001031289.2
IL-6	F: CCAAGGTGACGGAGGAGGAC R: CAGGTAGGTCTGAAAGGCGAAC	NM_204628.2
IL-1β	F: GCCCTCCTCCAGCCAGAAAG R: TGTAGCCCTTGATGCCCAGTG	NM_204524.2
TNF-α	F: TGACCGCCCAGTTCAGATGAG R: GCACCCCAGCAGGAAGAGG	XM_046900551.1

to overt clinical pathology, ultimately resulting in reduced feed conversion ratio, elevated mortality, and considerable economic losses (Wang et al., 2022). Given the pathological mechanisms and economic consequences outlined above, the development of safe and effective interventions to prevent and control LPS-induced hepatic inflammation is of urgent practical significance for safeguarding poultry health, ensuring the stability of poultry production, and maintaining food safety.

Currently, the routine prevention and treatment of inflammatory diseases in livestock and poultry rely primarily on antibiotics and chemically synthesized anti-inflammatory drugs. The widespread use of these agents has triggered a series of severe challenges, including bacterial antimicrobial resistance and drug residues in animal tissues (Chen et al., 2025; Cheng and Cheng, 2024). Accordingly, identifying efficacious, low-toxicity, residue-free natural bioactive substances as alternatives to facilitate the green and sustainable development of animal husbandry has become a research priority (Xing et al., 2023). Growing literature substantiates that flavonoids and phenolic phytochemicals confer dual anti-inflammatory and hepatoprotective benefits across multiple poultry liver disease models (Guo et al., 2026). Chicoric acid (**CA**) is a naturally occurring phenolic acid derived from Asteraceae plants, possessing pronounced anti-inflammatory, antioxidant, and immunomodulatory activities. Its hepatoprotective effects have been validated in rodent models, providing a theoretical foundation for its potential application in the prevention and control of inflammatory diseases in livestock and poultry (Ding et al., 2019; Peng et al., 2019; Yang et al., 2022).Nevertheless, systematic studies on the pharmacological properties and mechanisms of action of CA in poultry, particularly regarding its protective efficacy against LPS-induced hepatic inflammation and the underlying regulatory pathways, remain scarce at present. Considering the multi-target, multi-pathway anti-inflammatory characteristics of CA documented in existing research, the present study employed network pharmacology combined with molecular docking approaches to predict the potential targets and core signaling pathways through which CA exerts its effects, thereby establishing a theoretical basis for subsequent in vivo and in vitro validation experiments. This study aims to systematically elucidate the pharmacological mechanism by which CA alleviates LPS-induced hepatic inflammation in broilers.

Based on network pharmacology and molecular docking predictions, the anti-inflammatory and hepatoprotective effects of CA were evaluated in an LPS-induced broiler hepatic inflammation model using both in vivo and in vitro approaches. This study elucidates the pharmacological mechanism of CA and supports its development as a plant-derived, antibiotic-alternative hepatic protective agent.

Materials and methods

Materials and reagents

CA obtained from Chengdu Manster Biotechnology Co., Ltd. (Chengdu, China). LPS, 4% paraformaldehyde fixative, Dulbecco's modified Eagle medium: nutrient mixture F-12 (**DMEM/F12**), phosphate buffer saline (**PBS**), Hank's balanced salt solution (**HBSS**), and BCA protein assay kit were sourced from Beijing Solaibo Technology Co., Ltd. (Beijing, China). The enzyme-linked immunosorbent assay (**ELISA**) kits for interleukin-6 (**IL-6**), tumor necrosis factor-α (**TNF-α**), and interleukin-1β (**IL-1β**) were all purchased from Shanghai Mlbio Co., Ltd. (Shanghai, China). All DNA primers used in this study were synthesized by Sangon Biotech Co., Ltd. (Shanghai, China) and are listed in Table 1. The total RNA extraction reagents, ancillary reagents, StarScript Pro All-in-one RT Mix with gDNA Remover, and 2 × RealStar Universal SYBR qPCR Mix were purchased from Beijing Kangrun Biotech Co., Ltd. (Beijing, China). Rabbit polyclonal antibodies against TLR4 (19811-1-AP), phospho-p38 MAPK (Thr180/Tyr182, 28796-1-AP), phospho-TAK1 (Thr187, 28958-1-AP), TAK1 (12330-2-AP), p38 (14064-1-AP) and vinculin (26520-1-AP), together with the HRP-conjugated goat anti-rabbit IgG (H+L) secondary antibody (SA00001-2), were obtained from Proteintech Group (Wuhan Sanying Biotechnology Co., Ltd., Wuhan, China).

Network pharmacology analysis

A multi-database cross-verification strategy was adopted to systematically predict potential targets of CA to improve the reliability and coverage of prediction results. All annotations obtained from SwissTargetPrediction (http://www.swisstargetprediction.ch/), PharmMapper (http://www.lilabecust.cn/pharmmapper/), SuperPred (https://prediction.charite.de/) and SEA (https://sea.bkslab.org/) databases used in this study correspond to human-derived genetic data. The two-dimensional chemical structure of CA was retrieved from the PubChem database (https://pubchem.ncbi.nlm.nih.gov/). The acquired structure was separately submitted to the four complementary target prediction platforms mentioned above. Target gene symbols were converted via the UniProt database (http://www.uniprot.org/), and duplicates were eliminated to establish a human-derived candidate target set of CA.

Using "Hepatic Inflammation" as the search term, hepatic inflammation-related disease targets were retrieved from the OMIM (https://omim.org/) and GeneCards (https://www.genecards.org/) databases. For GeneCards database, genes were filtered with a Relevance Score $\geq$ 30; for OMIM database, only entries with clear disease-gene association evidence were retained, while genes with low-grade evidence and ambiguous annotations were excluded. All screened targets were standardized to standard human gene symbols through UniProt, merged, and de-duplicated to construct a dataset of human-derived hepatic inflammation-associated disease targets. It should be noted that the network pharmacology analysis in this part represents cross-species bioinformatic prediction, which is applied to screen candidate pathway hypotheses. Subsequent in-vivo and in-vitro experiments using avian samples will be performed for experimental validation.

The Venny 2.1.0 online tool (https://bioinfogp.cnb.csic.es/tools/venny/) was used to identify overlapping targets between CA candidate targets and hepatic inflammation-related targets. The standardized datasets of CA candidate targets and hepatic inflammation disease targets were separately uploaded to the platform, and intersection genes were screened via set operation as potential therapeutic targets of CA against hepatic inflammation.To clarify the interaction relationships among overlapping targets, the list of intersection genes was imported

into the STRING database (https://string-db.org/). The species was set as *Homo sapiens*, the medium confidence threshold was defined as ≥ 0.4, and all other parameters were kept as default to construct a protein–-protein interaction (**PPI**) network. The exported network data were imported into Cytoscape 3.10.2 software for topological analysis and visualization. Nodal parameters including betweenness centrality, degree centrality and closeness centrality were utilized as core indicators to screen key candidate targets for subsequent pathway enrichment and mechanistic exploration.

GO and KEGG pathway enrichment analysis

Gene ontology (**GO**) functional annotation and Kyoto Encyclopedia of Genes and Genomes (**KEGG**) pathway enrichment analyses were performed on overlapping targets to systematically elucidate the underlying molecular mechanisms by which CA alleviates hepatic inflammation. The standardized gene list was submitted to the DAVID database (https://davidbioinformatics.nih.gov/), with species specified as Homo sapiens and all remaining analytical parameters maintained at default settings.

GO and KEGG pathway enrichment analyses were conducted on the screened candidate targets to obtain significantly enriched terms. The GO enrichment bar chart and KEGG enrichment bubble chart were constructed using the online visualization tool Bioinformatics. The GO bar chart illustrated enriched terms and corresponding gene counts of biological process (**BP**), cellular component (**CC**), and molecular function (**MF**). For the KEGG bubble chart, GeneRatio was set as the abscissa and pathway names as the ordinate. The size of bubbles represented the number of enriched genes, and bubble color corresponded to $-\log_{10}$(p-value), so as to visualize gene counts and statistical significance of enriched pathways.

Molecular docking

The three-dimensional structure of CA was downloaded from PubChem, and crystal structures of target proteins were obtained from the RCSB Protein Data Bank (https://www.rcsb.org/). Since no experimentally-determined chicken TLR4 and TAK1 crystal structures are available in the RCSB-PDB database, human crystal structures were adopted as docking templates (PDB IDs: TLR4-MD2: 3FXI; TAK1: 2EVA; p38α: 1P38; JNK1: 3OYM; JNK2: 3NPC). Water molecules and co-crystallized native ligands were removed using PyMOL, and processed files were saved in PDB format. Polar hydrogens were added to protein structures using AutoDockTools 1.5.7 for docking preparation.

Grid-boxes were placed at the known ligand-binding pocket of each target. Center coordinates and dimensions (Å): TLR4 (−22.1, 18.4, 29.7), (26, 26, 26); TAK1 (10.2, −3.8, 21.5), (24, 24, 24); p38α (1.4, 12.6, 19.2), (24, 24, 24); JNK1 (4.8, 15.1, 22.3), (24, 24, 24); JNK2 (−5.7, 8.2, 17.5), (24, 24, 24). Exhaustiveness was set to 8. Re-docking-based RMSD validation was not performed in this study. AutoDock Vina was applied to simulate molecular docking between CA and processed target proteins and calculate corresponding binding affinities. Finally, PyMOL was employed to visualize the binding conformation of CA within the active pocket of target proteins.

Experimental animals

In this experiment, twenty-four 1-month-old Chinese White-feather broilers in good health were utilized. All broilers were housed under controlled environmental conditions starting at one day of age and had unrestricted access to basal diet and drinking water throughout the trial. The temperature was set at 35°C during the initial 3-day acclimatization phase, followed by a gradual reduction to 28–30°C over 14 days, and was finally maintained at 25°C until the endpoint. The broiler management and experimental protocols were approved by the Animal Ethics Committee of Hebei Agricultural University (approval number: 2022026). Broilers were humanely euthanized via cervical dislocation post-trial.

Pharmacodynamic study

Twenty-four healthy 1-month-old White-feather broilers were selected and randomly divided into four groups: control group, positive group, model group and administration group. Dexamethasone (**DXM**) served as the positive control. Broilers in the CA administration group were intragastrically administered CA at 15 mg/kg twice daily (morning and evening) for five consecutive days. Broilers in the DXM positive control group received DXM intramuscularly at 2 mg/kg twice daily for five consecutive days. Broilers in the control and model groups received an equal volume of vehicle by gavage twice daily over the same 5-day period to standardize handling and gavage stress across all groups. At the end of the 5-day pre-treatment period, intraperitoneal injection was performed. The control group was injected with an equal volume of sterile normal saline, while the model, DXM positive control, and CA administration groups received LPS (1 mg/kg). Twelve hours later, wing vein blood and liver tissue samples were collected. Blood samples were placed obliquely for 2 hours, and the separated serum as well as liver tissues were stored at −80°C. The levels of TNF-α, IL-1β and IL-6 in serum and liver tissues were detected using commercial chicken ELISA kits following standard operating procedures.

Histopathological analysis

Representative liver tissue samples were fixed in 4% paraformaldehyde (in PBS), routinely processed, and embedded in paraffin wax. Sections were stained with hematoxylin and eosin (**H&E**), and histopathological morphology was evaluated using a light microscope. Representative photomicrographs were captured for documentation.

Cell culture and cytotoxicity assay

The Leghorn Male Hepatoma (**LMH**) cell line (Beina, Shanghai, China) was cultured at 37 °C in a humidified incubator with 5 % CO_2 using DMEM/F12 (1:1) supplemented with 10 % fetal bovine serum (**FBS**). 80% of cells were subcultured at a ratio of 1:2. Logarithmic-phase LMH cells were seeded into a 96-well plate at a density of 5×10^4 cells per well and treated with CA at concentrations of 100, 200, 400, 600, and 1000 μmol/L for 24 h. Absorbance in each well was measured at 570 nm using a microplate reader following the MTT assay. Calculate the cell survival rate: cell survival rate (%) = ($D_{570\ nm}$ in the administration group/$D_{570\ nm}$ in the control group) × 100%.

Cytotoxicity assay of LPS

LMH cells in the logarithmic growth period were inoculated into 96-well plates at the rate of 5×10^4/well, and LPS was used as the modeling agent. Different concentrations of LPS solutions were added to incubate for 12 h: 0 (control group), 0.2, 0.5, 1, 2, 5, 10, 20, 50, 100, and 200 μg/mL, respectively. Cells in the control group were treated with an equal volume of buffer solution. Following the MTT assay, absorbance was measured at 570 nm using a microplate reader.

Evaluation of CA-mediated protection and recovery in LPS-challenged LMH cells

Logarithmic-phase LMH cells were seeded into 96-well plates at a density of 5×10^4 cells/well and assigned to the following groups: control group, LPS group (at the optimal concentration determined by prior screening), positive (DXM, 300 ng/mL) group, and CA-treated (40–600 μmol/L) groups. In the protection assay, non-control cells were pretreated with CA or DXM for 24 h before LPS stimulation. In the recovery assay, cells were first exposed to LPS and then treated with CA

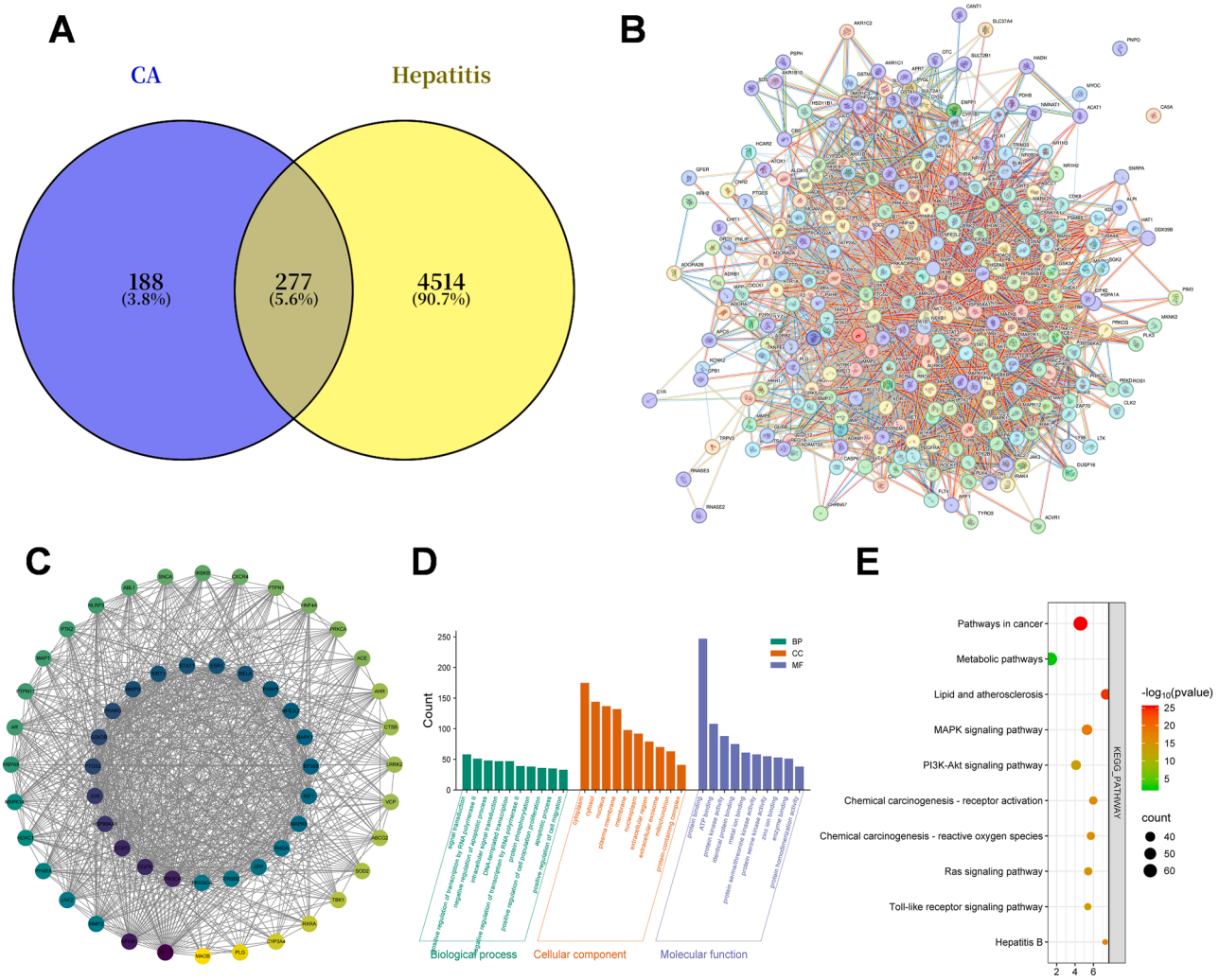

Fig. 1. Screening of potential targets of CA and molecular docking verification. (A) Venn diagram of CA and liver inflammation target overlaps. (B) Intersection target protein interaction network. (C) Core target protein interaction network. (D) GO enrichment analysis plot. (E) KEGG pathway enrichment analysis.

or DXM for 24 h. The control group received only HBSS throughout the entire incubation period. In both assays, cell viability was assessed using the MTT assay (570 nm), and absorbance was measured to calculate cell survival rates. Additionally, cellular morphology was evaluated by inverted light microscopy, and nuclear morphological features were quantitatively analyzed by fluorescence microscopy following DAPI staining.

Quantitative real-time polymerase chain reaction (qRT-PCR)

Total RNA was extracted from liver tissue and LMH cells using a commercial kit according to the manufacturer's instructions. The concentration and purity of the total RNA were determined by the UV-Vis spectrophotometer, followed by cDNA synthesis. The qRT-PCR conditions were as follows: 95°C for 2 min (initial denaturation); 40 cycles of 95°C for 10 s (denaturation) and 60°C for 30 s (annealing/extension). The β-actin gene was used as the internal reference gene. Quantitative real-time PCR was performed using the 2ˆ(−ΔΔCt) relative quantification method. This method assumes that the amplification efficiency of each primer pair is close to 100%.

Western blot

LMH cells were seeded in 6-well plates and treated according to the aforementioned grouping strategy to evaluate the protective effect of CA on LMH cells. After LPS incubation, total cellular protein was extracted, and its concentration was determined using a BCA protein assay kit. Equal amounts of protein were separated by 10% SDS-polyacrylamide gel electrophoresis (SDS-PAGE) and transferred onto polyvinylidene difluoride (PVDF) membranes. Separate membranes were used for the detection of TAK1, p-TAK1, p38, and p-p38. These membranes were blocked with 5% bovine serum albumin at room temperature for 1 h, followed by overnight incubation at 4 °C with primary antibodies against TAK1 (1:500), p-TAK1 (1:5000), p38 (1:2000), and p-p38 (1:2000). For TLR4 and vinculin detection, another set of PVDF membranes were blocked with 5% bovine serum albumin at room temperature for 1 h and incubated overnight at 4 °C with primary antibody against TLR4 (1:500). After signal acquisition, the blots were washed thoroughly with TBST and immersed in boiling distilled water for 4 min for stripping. After cooling and extensive washing with TBST, complete removal of residual antibody was verified by ECL exposure prior to re-blocking. The membranes were re-blocked and incubated overnight at 4 °C with primary antibody against vinculin (1:5000). After each primary antibody incubation, the membranes were incubated with an HRP-conjugated goat anti-rabbit secondary antibody (1:10000) at room temperature for 2 h. Protein expression was detected using an enhanced chemiluminescence (ECL) substrate. Band intensities were quantified using ImageJ software.

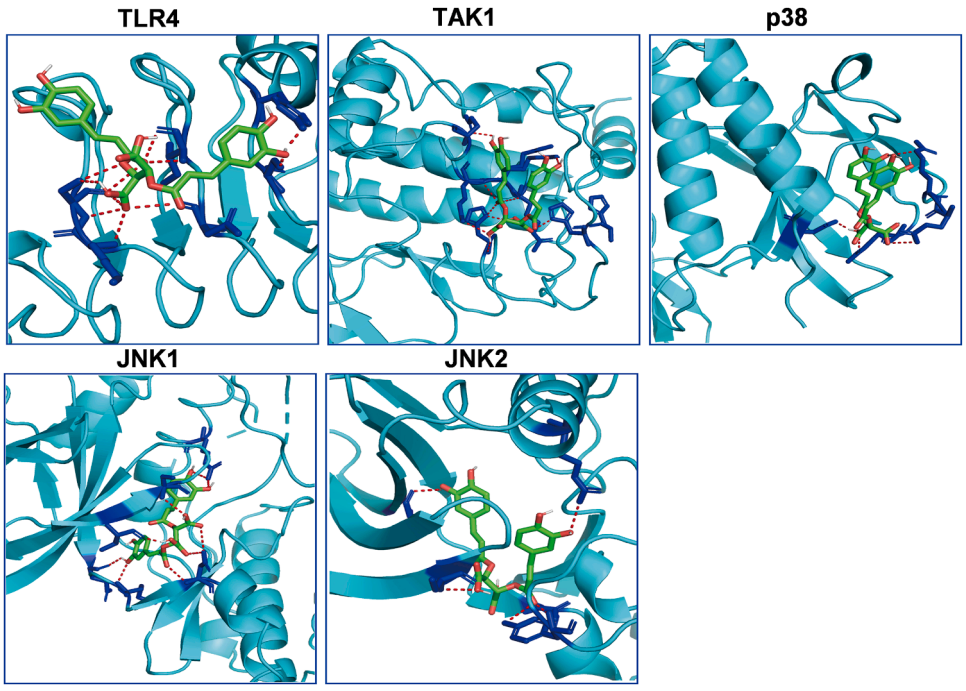

Fig. 2. Molecular docking of key proteins in the CA and TLR4/MAPK signaling pathways.

Statistical analysis

All data are presented as mean ± standard deviation (SD). Statistical analyses were performed using GraphPad Prism 10.0 and SPSS 20.0. The assumptions of one-way ANOVA were verified by Shapiro–Wilk test for normality and Levene's test for homogeneity of variance. A biological replicate represents one broiler (in vivo) or an independent LMH cell culture batch (in vitro). One-way ANOVA followed by Tukey's HSD test was used when assumptions were met. $P < 0.05$ was considered statistically significant and $P < 0.01$ highly significant.

Results

Network pharmacology prediction results

A multi-database cross-validation strategy was applied. After standardization and deduplication using UniProt, a non-redundant dataset of candidate CA targets was established, containing a total of 465 originally predicted targets. Meanwhile, hepatic inflammation-related targets were systematically retrieved from the OMIM and GeneCards databases and processed following the same standard procedures, yielding 4791 disease-associated genes. Venn analysis revealed 277 overlapping genes between CA candidate targets and hepatic inflammation-related genes (Fig. 1**A**). These intersecting genes were imported into the STRING database to construct a PPI network, which consisted of 277 nodes and 3968 interaction edges (Fig. 1**B**). For topological characterization and core target identification, the PPI network data were visualized and analyzed via Cytoscape 3.10.2 (Fig. 1**C**). The color gradient of nodes represented the Degree value: darker color indicated a higher Degree value.

GO and KEGG pathway enrichment analysis

GO enrichment yielded 187 significant terms: 86 BP, 50 CC, 51 MF. The top 10 terms of each category (Fig. 1**D**) mainly referred to signal transduction, transcriptional regulation by RNA polymerase II, negative regulation of apoptotic process, and protein phosphorylation in biological processes; nucleus, mitochondrion, cytoplasm and protein complex in cellular components; as well as protein binding, serine/threonine kinase activity, ATP binding, metal ion binding and protein phosphatase binding in molecular functions.

A total of 153 pathways were significantly enriched by KEGG analysis (Fig. 1**E**). The MAPK signaling pathway showed relatively high enrichment, and its core targets were selected for further mechanistic and pharmacodynamic verification. The Toll-like receptor signaling pathway was also significantly enriched. These pathways collectively form the molecular network underlying the anti-inflammatory effect of CA on hepatic inflammation.

Table 2
Binding affinities and key hydrogen-bonding residues of CA with TLR4/MAPK pathway proteins.

Small Molecule	Proteins	Affinity (kcal/mol)	Interacting Residues with H-bond
CA	JNK1	−9.0	Arg69, Ser34, Ile32, Glu109, Met111, Asn114
	JNK2	−9.1	Aeg69. Ala53, Ser34, Asn114, Tyr185
	p38	−7.1	Arg5, Asp88, Arg23, Glu4
	TAK1	−8.8	Glu231, Lys227, His117, His468, Arg225, Arg226
	TLR4	−6.9	Tyr191, Ile218, Ser189, Ser240, Lls239, Asn216

Molecular docking of CA with core targets

Molecular docking was performed to predict potential interactions between CA and core hub proteins (Fig. 2), with detailed results shown in Table 2. Docking simulations suggested favorable interactions between CA and TLR4, TAK1, p38, JNK1 and JNK2, with binding energies ranging from −6.9 to −9.1 kcal/mol.

Effects of CA on LPS-induced hepatic histopathological changes

To assess the impact of CA on LPS-induced hepatic inflammation, histomorphological changes in broiler liver tissues were examined by

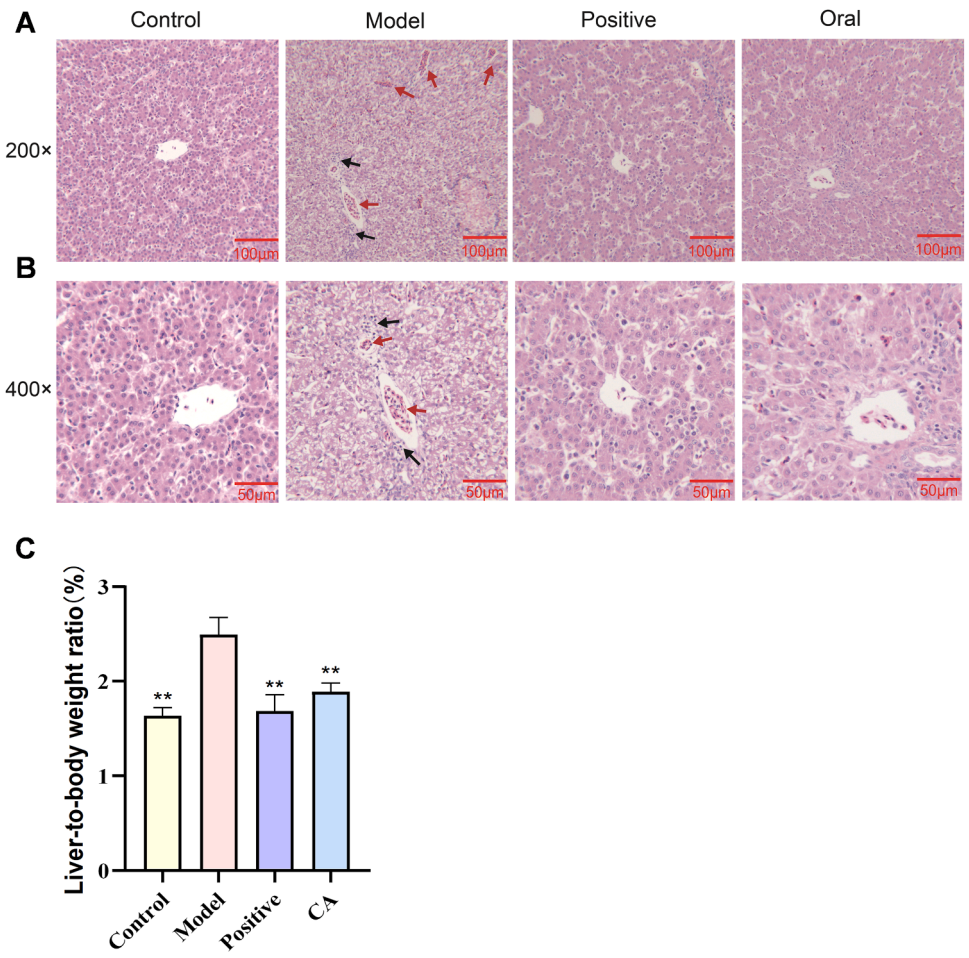

Fig. 3. CA attenuates LPS-induced hepatic tissue damage in broilers. (A) Observation results of H&E staining in the liver tissue of broilers. Scale: 50 μm and (B) 100 μm. Note: red arrow: hyperemia; black arrow: inflammatory cells. (C) Liver-to-body weight ratio in broilers. Data are presented as mean ± SD (n = 6). **p < 0.01, vs. model group.

H&E staining, and the liver-to-body weight ratio was determined. H&E staining analysis (Fig. 3**A-B**) revealed distinct pathological alterations in the model group, including disorganized hepatic cord arrangements, vacuolar degeneration of hepatocytes, marked congestion in sinusoidal spaces and perivascular areas, and prominent inflammatory cell infiltration. In contrast, the control group showed well-aligned hepatocytes with intact hepatic cords and hepatic sinusoids, showing no pathological abnormalities. Compared to the model group, the CA treatment group showed significant improvements: hepatocyte vacuolar degeneration was markedly reduced, sinusoidal congestion was alleviated, and only minor residual inflammatory cell infiltration was observed. The positive group showed comparable efficacy to the CA-treated groups. Analysis of the liver-to-body weight ratio revealed a significant increase in the model group compared with the other groups ($P < 0.01$; Fig. 3**C**), suggesting that LPS-induced inflammation led to a marked elevation in relative liver weight.

CA attenuates LPS-induced hepatic inflammation in broilers

To systematically evaluate the anti-inflammatory potential of CA against LPS-induced hepatic inflammation in broilers, ELISA was adopted to detect the contents of pivotal pro-inflammatory cytokines TNF-α, IL-1β and IL-6, in serum and liver homogenates. As shown in Fig. 4A-C, LPS exposure remarkably increased the levels of these three cytokines in serum and hepatic tissues relative to the control group ($P < 0.01$), confirming the establishment of inflammatory injury. Both CA intervention and positive drug treatment markedly restrained the abnormal release of pro-inflammatory cytokines when compared with the model group. The inhibitory capacity of CA against serum IL-6 and IL-1β was equivalent to that of the positive control group. CA also exerted prominent anti-inflammatory activity in hepatic tissues and effectively reduced the accumulation of inflammatory mediators. qRT-PCR was further conducted to explore the regulatory mechanism of CA on LPS-triggered hepatic inflammation by detecting mRNA expression of core genes involved in the TLR4/MAPK signaling pathway. As illustrated in Fig. 5, the transcriptional levels of TLR4, MYD88, TAK1, JNK1 and JNK2 were sharply upregulated in the model group ($P < 0.01$), implying excessive activation of the TLR4/MAPK inflammatory signaling pathway. CA administration effectively reversed the elevated expression of these pathway-related genes ($P < 0.01$). These results indicate that CA alleviates LPS-induced hepatic inflammatory damage in broilers via suppressing pro-inflammatory cytokine secretion and inhibiting the abnormal activation of the TLR4/MAPK signaling cascade.

Effect of CA pretreatment or treatment on cell viability in LPS-induced LMH cells

As shown in Fig. 6A, cell viability remained above 90% across all tested concentrations of CA, indicating the absence of cytotoxic effects within this concentration range. As illustrated in Fig. 6B, LPS induced a dose-dependent reduction in cell viability. Based on these results, an LPS concentration of 50 μg/mL (cell viability: 69.8%) was selected as the standard challenge dose for subsequent experiments. In the protection

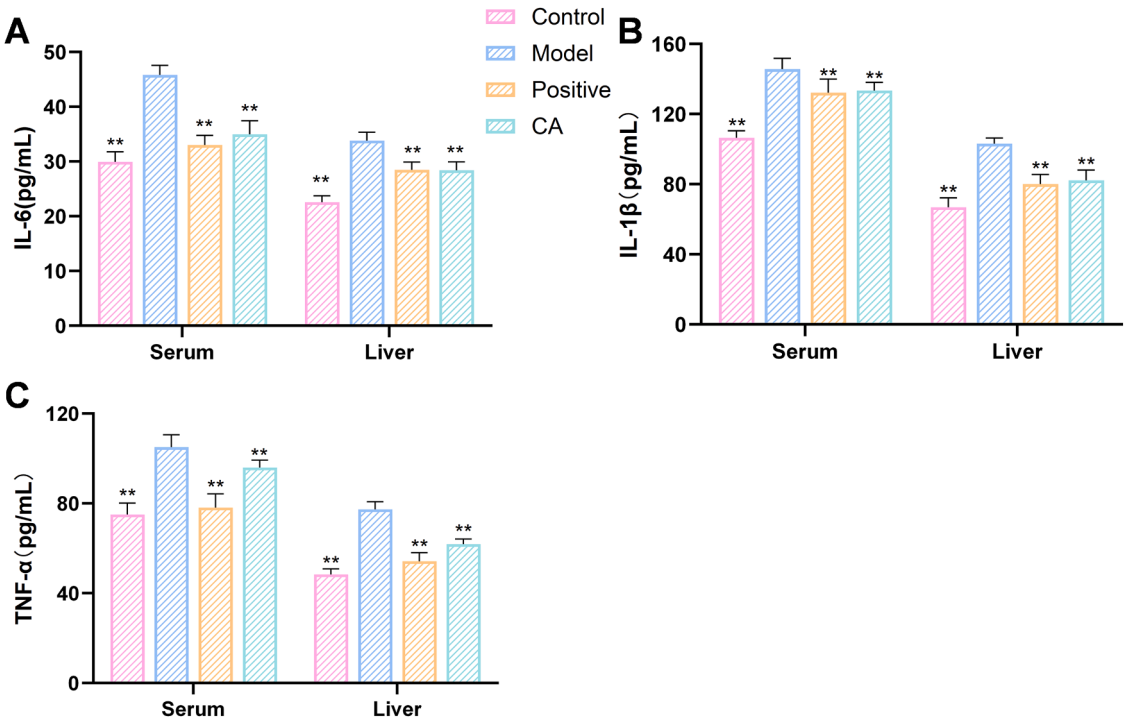

Fig. 4. Effect of CA on pro-inflammatory cytokine levels in LPS-challenged broilers. The level of IL-6 (A), IL-1β (B), and TNF-α (C) in serum and liver. Data are presented as mean ± SD (n = 6). *p < 0.05 and **p < 0.01, vs. model group.

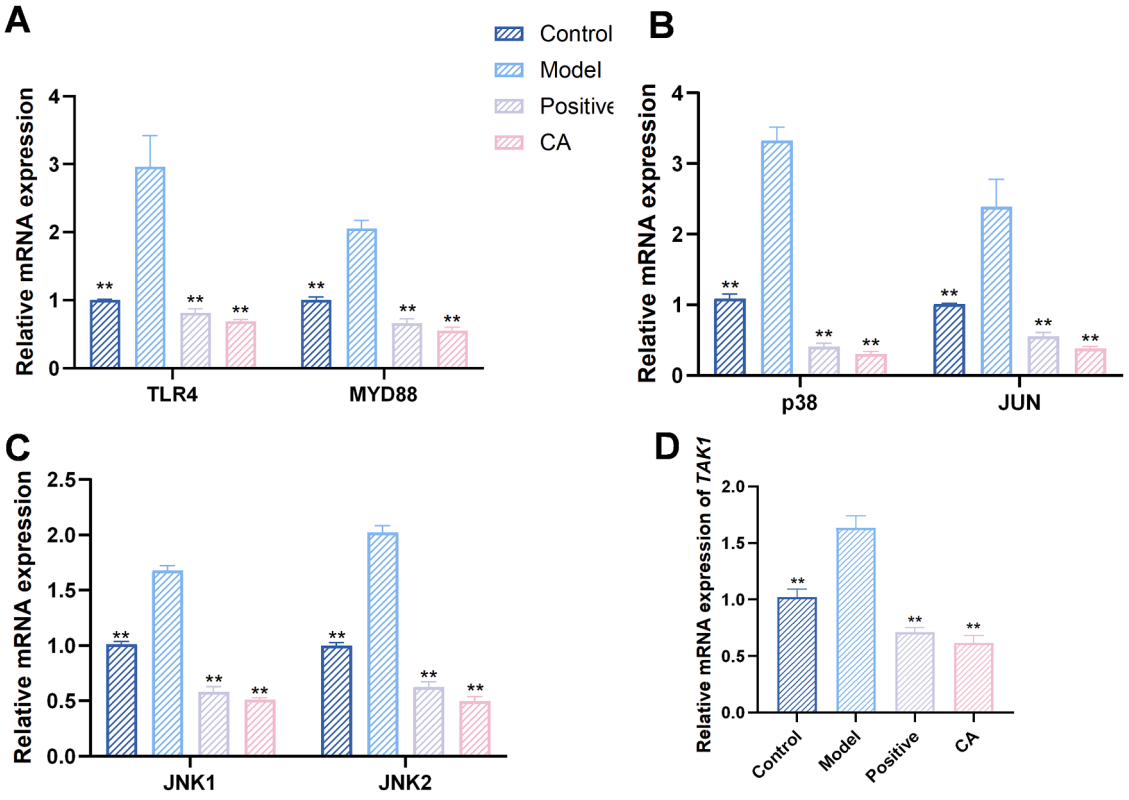

Fig. 5. CA suppresses LPS-induced upregulation of key genes in the TLR4/MAPK signaling pathway. qRT-PCR analysis of hepatic (A) TLR4/MYD88, (B) p38/JUN, (C) JNK1/JNK2 and (D) TAK1 mRNA levels. Data are presented as mean ± SD (n = 6). *p < 0.05 and **p < 0.01, vs. model group.

assay, preincubation of LMH cells with CA (50–600 μmol/L) before LPS exposure resulted in a concentration-dependent increase in cell viability, with maximal protection observed at 400 μmol/L compared to the LPS-only control (Fig. 6C). This concentration was therefore selected as the optimal dose of CA for further mechanistic studies. Morphological analysis confirmed that LPS treatment markedly suppressed cell

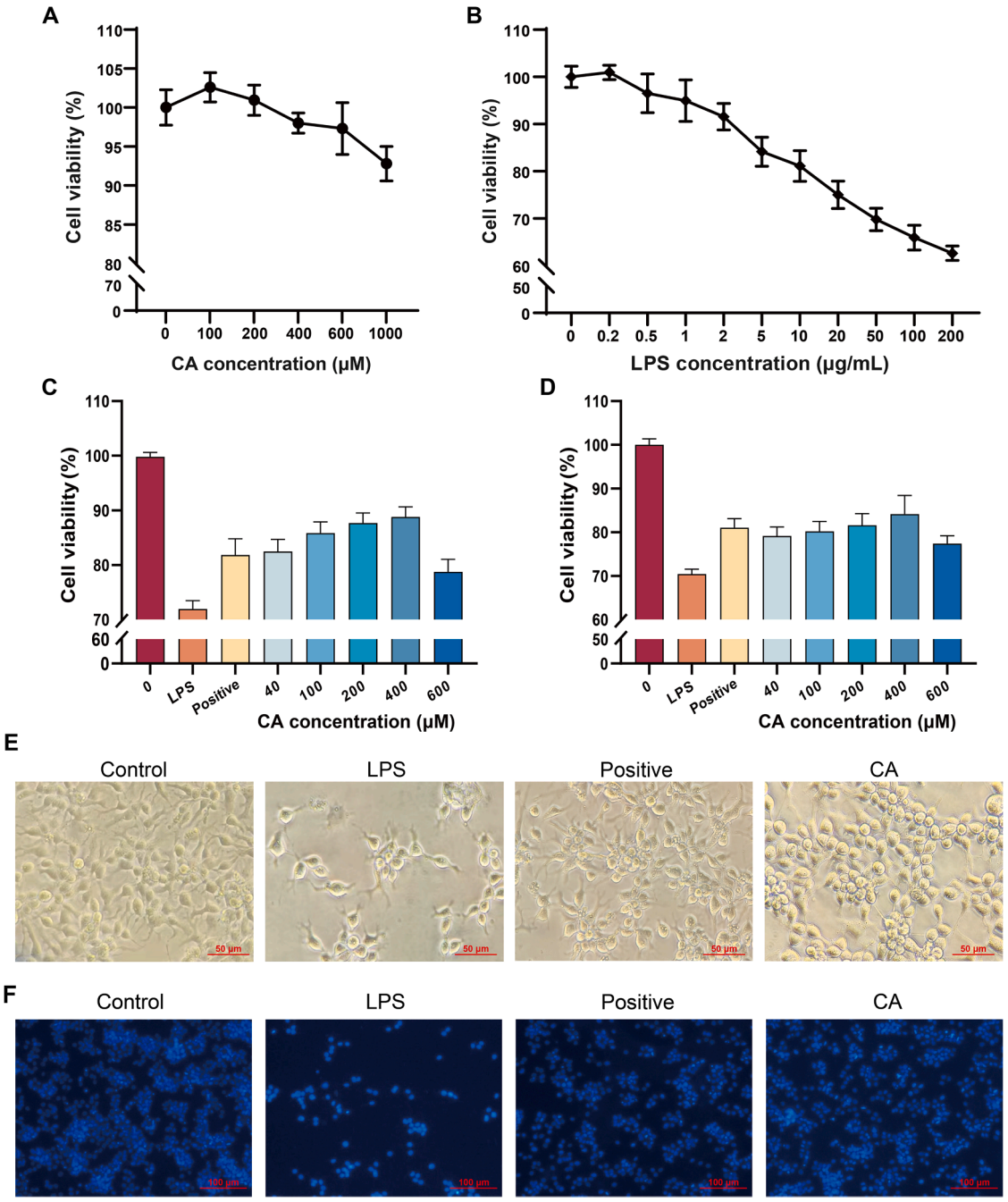

Fig. 6. CA alleviates LPS-induced cytotoxic and inflammatory responses in LMH cells. (A) Cytotoxicity assessment of CA in LMH cells. (B) Preliminary screening of LPS concentrations in LMH cells. (C) Effect of CA pretreatment on LMH cell viability following LPS challenge. (D) Effect of post-LPS CA treatment on recovery of LMH cell viability. (E) CA preserves LMH cell morphology and density against LPS-induced injury. Scale: 50 μm. (F) DAPI staining analysis of CA-mediated protection in LPS-stimulated LMH cells. Scale: 100 μm. Data are presented as mean ± SD (n = 6).

proliferation, showing widened intercellular spaces and fewer cells per field, while CA-treated cells maintained normal density similar to controls (Fig. 6**E-F**). When administered following LPS challenge within the identical concentration range, CA still exerted obvious cytoprotective effects against LPS-induced cytotoxicity, albeit with reduced potency. At the 400 μmol/L concentration, cell viability reached 84.14% (Fig. 6**D**).

CA attenuates LPS-induced pro-inflammatory signaling in LMH cells with concomitant downregulation of TLR4/MAPK pathway components

qRT-PCR results demonstrated that LPS challenge markedly elevated the mRNA levels of pro-inflammatory cytokines including IL-6, TNF-α and IL-1β, as well as key genes involved in the TLR4/MAPK signaling pathway relative to the control group ($P < 0.01$, Fig. 7**A–F**). Pretreatment with either CA or DXM effectively reversed this LPS-mediated upregulation. Both CA and DXM significantly decreased the transcript abundance of these inflammatory and pathway genes after LPS stimulation.

Western blot analysis further verified the alterations at the protein level in LMH cells. Repeated attempts failed to yield stable phosphorylated JNK bands; therefore, only TLR4, TAK1 and p38 were detected by Western blot. LPS stimulation elevated total TLR4 protein abundance and enhanced phosphorylation of TAK1 and p38. These molecular changes were markedly attenuated by CA pre-treatment ($P < 0.05$,

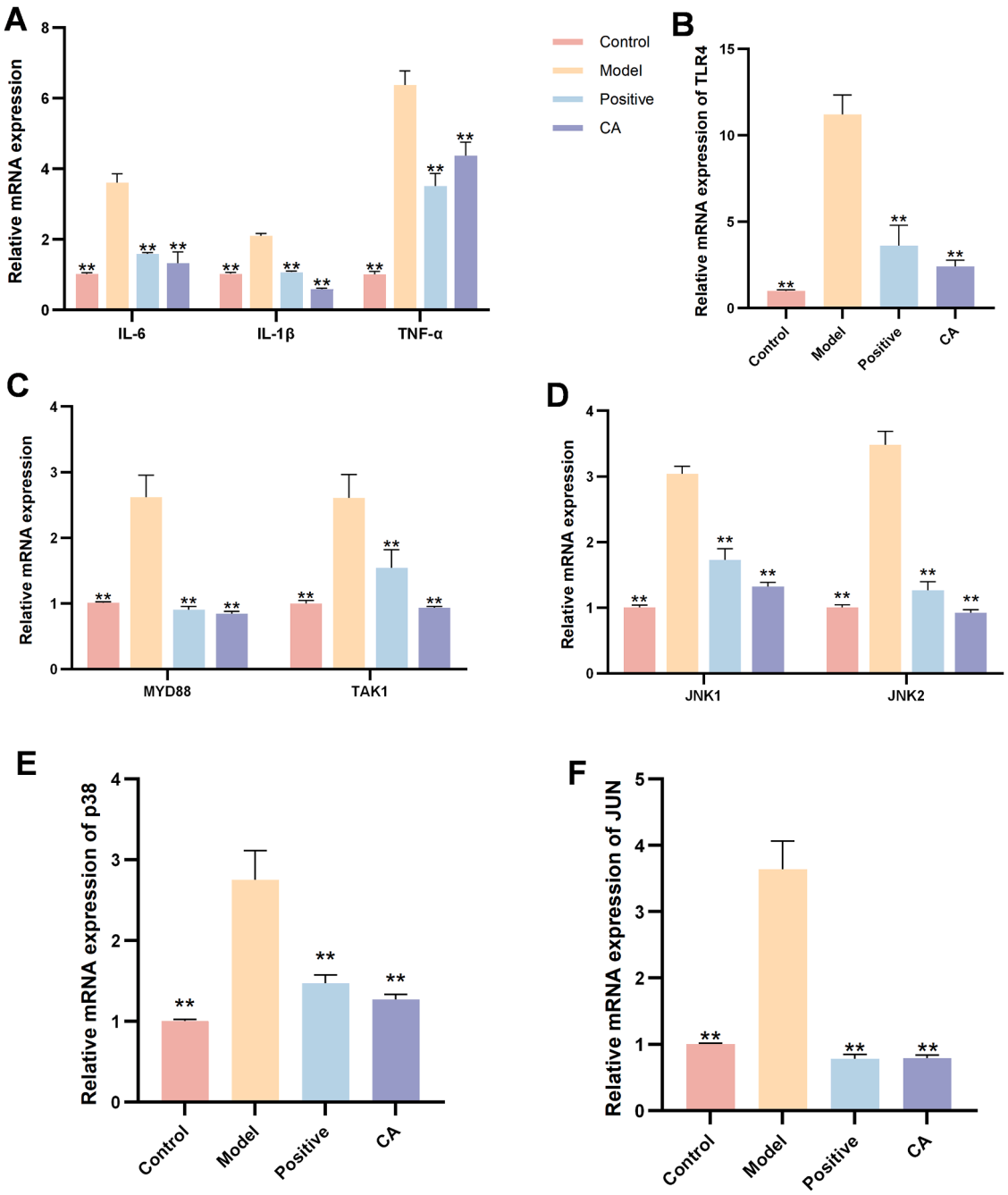

Fig. 7. CA pretreatment downregulates the transcriptional levels of LPS-induced inflammatory-related genes in LMH cells. (A) IL-6, IL-1β, and TNF-α mRNA levels, (B) TLR4, (C) MYD88/TAK1, (D)JNK1/JNK2, (E) p38, (F) JUN. Data are presented as mean ± SD (n = 6). *p < 0.05 and **p < 0.01, vs. model group.

Fig. 8), whereas total-TAK1 and total-p38 protein abundances remained unaltered. Vinculin was used as the loading control. A schematic illustration summarizing the mechanism by which CA mitigates LPS-triggered inflammatory signaling in LMH cells is presented in Fig. 9.

Discussion

Under intensive broiler production systems, broilers exhibit rapid growth rates, and the liver, as the central organ responsible for systemic metabolism and detoxification, is highly susceptible to inflammatory injury. Hepatic inflammation disrupts nutritional metabolism and compromises immune function; therefore, the prevention of hepatic lesions has become a top priority in modern, high-efficiency poultry production. Driven by the urgent need for alternatives to antibiotics, plant-derived anti-inflammatory compounds such as polyphenols, flavonoids, and terpenoids have been extensively investigated for their immunomodulatory activities (Ivanova et al., 2024). The liver plays a critical role in innate immunity, and its histomorphological characteristics serve as important indicators for evaluating the health status of the organism (Zhang et al., 2023) When intestinal barrier integrity is compromised, bacterial endotoxin LPS can translocate into the systemic circulation and induce hepatic inflammation (Wang et al., 2026). Given that LPS consistently and reliably induces inflammatory responses in poultry, a finding well corroborated by existing literature, the present study employed LPS to establish a broiler hepatic inflammation model. LPS stimulates hepatic macrophages to release pro-inflammatory cytokines, upregulating the expression of TNF-α, IL-6, and IL-1β. This not only represents a classical hallmark of innate immune activation but also

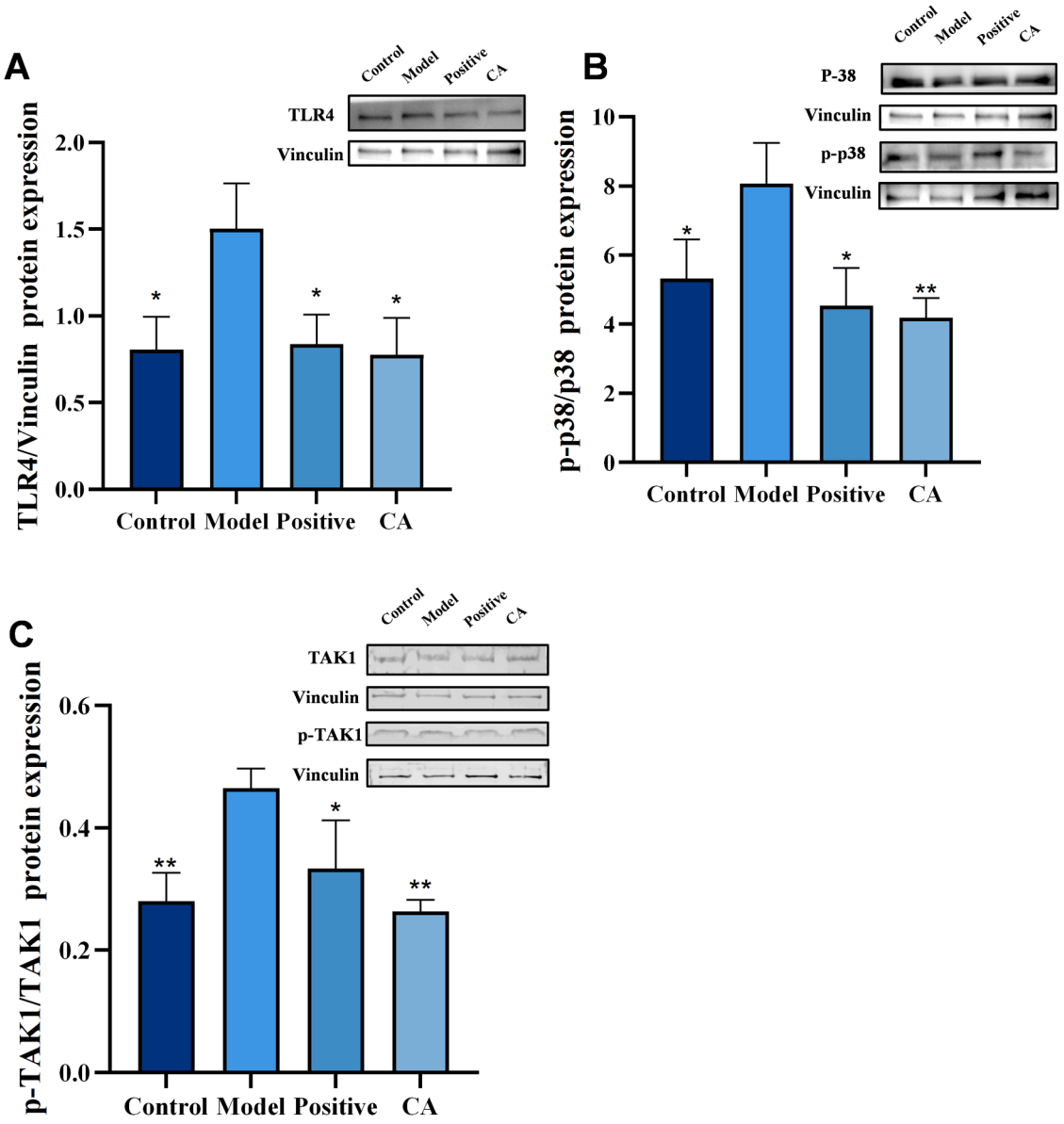

Fig. 8. CA reduces LPS-induced elevation of TLR4, phosphorylated TAK1, and phosphorylated p38 protein levels in LMH cells. Protein expression was determined by Western blotting. Vinculin served as the loading control. Data are presented as mean ± SD (n = 3). *p < 0.05 and **p < 0.01 versus the model group.

constitutes a critical trigger leading to metabolic disturbances and hepatocellular damage in poultry (Liao and Lin, 2011). specifically manifested as oxidative stress, disruption of hepatic lobular architecture, inflammatory cell infiltration, and hepatocellular vacuolar degeneration (Huynh et al., 2020; Xu et al., 2021; Zhang et al., 2024). In the present study, the livers of broilers in all LPS-treated groups exhibited inflammatory cell infiltration. H&E staining revealed disorganized hepatic cords, central venous congestion, and hepatocellular vacuolar degeneration.

Our results demonstrated that CA treatment markedly ameliorated LPS-induced hepatic pathological injury and reduced the levels of inflammatory mediators in serum and liver tissue. Consistent with previous studies on natural active substances (Zheng et al., 2026), CA exhibited stable anti-inflammatory activity and effectively inhibited the secretion of pro-inflammatory cytokines such as TNF-α and IL-1β. Notably, CA modulated MAPK-related signaling molecules, indicating that its anti-inflammatory effects are predominantly mediated through the MAPK pathway. Network pharmacology and molecular docking analyses identified TLR and MAPK signaling as the top pathways enriched for CA targets, with TLR4, JNK and p38 as core predicted molecules. Notably, GO enrichment showed CA candidate targets were strongly linked to basal metabolic processes including citrate metabolism, the tricarboxylic acid cycle and carbohydrate metabolism, while inflammatory terms were not highly enriched. This implies CA may regulate both inflammation and host metabolism, and its metabolic effects merit further exploration. It should be emphasized that many of these predicted targets correspond to general metabolic enzymes. Since our experimental model was specifically constructed to evaluate LPS-triggered hepatic inflammatory injury, we prioritized experimental validation of inflammatory-related TLR/MAPK signaling rather than metabolic phenotypes. These metabolic-related enrichments remain purely computational outputs and have not been functionally tested in the current study. In addition, molecular docking in this study adopted human TLR4 and TAK1 crystal structures as templates, because chicken crystal structures of these two proteins are unavailable in PDB. This cross-species docking is only an in-silico prediction tool and cannot fully recapitulate native protein–ligand interactions in chicken. Moreover, network pharmacology serves as cross-species bioinformatic prediction

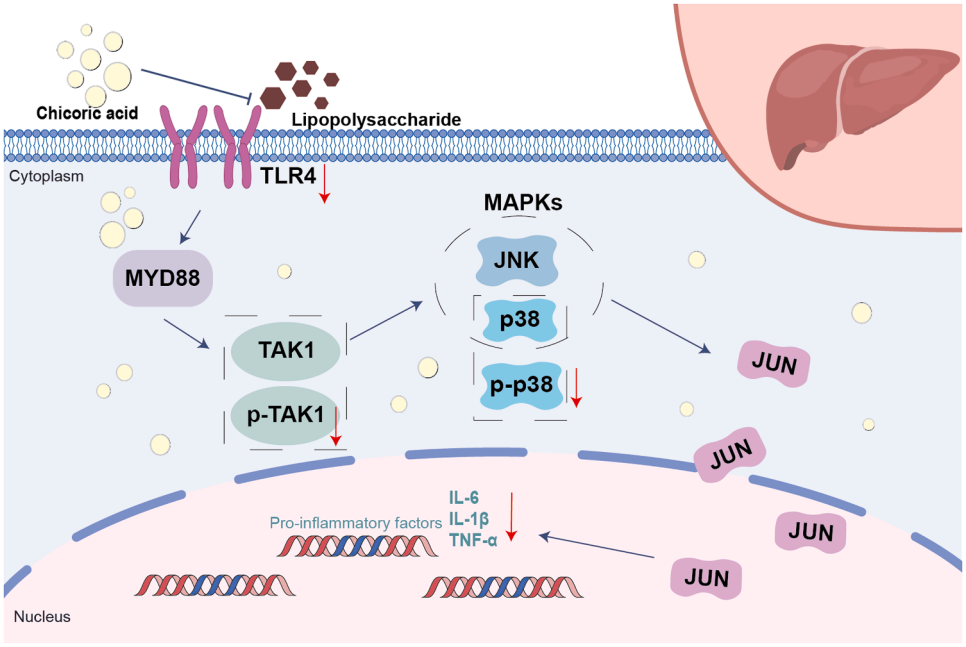

Fig. 9. Schematic illustration of the attenuation of LPS-induced pro-inflammatory signaling in LMH cells by CA.

for candidate pathway hypotheses validated by our avian in vivo and in vitro assays, and molecular docking merely yields in-silico predictions rather than proof of physical protein–ligand binding. The docking results therefore should be interpreted with caution.

TLR4 serves as a core pattern recognition receptor for LPS sensing and occupies a pivotal position in the pathogenesis of hepatic inflammation across multiple animal species. In poultry, elevated TLR4 mRNA expression is repeatedly linked to LPS-triggered inflammation, oxidative stress, and metabolic disorder (Chen et al., 2022). Following LPS binding, TLR4 recruits the adaptor protein MyD88 to launch an intracellular signaling cascade, which ultimately promotes the transcription and secretion of pro-inflammatory cytokines (Liu et al., 2024; Zhang et al., 2024). Molecular docking in the present study suggested potential favorable interactions between CA and the TLR4 protein, implying that CA may interfere with LPS recognition and subsequent receptor activation. Quantitative real-time PCR verified that CA treatment markedly attenuated LPS-elicited upregulation of TLR4 and MyD88 mRNA in broiler liver. In vitro assays further demonstrated that CA pretreatment lowered mRNA abundances of TLR4, MyD88, and major pro-inflammatory cytokines in LPS-stimulated chicken hepatoma cells. These observations align with prior reports. For example, in a mouse model of Parkinson's disease, CA decreased TNF-α and IL-1β release and alleviated neuronal injury via inhibition of the TLR4/MyD88/NF-κB cascade (Wang et al., 2022). Likewise, in high-fat diet-induced obese mice, CA downregulated TNF-α and IL-6 expression and mitigated hepatic steatosis and inflammation (Xiao et al., 2013), further supporting the central contribution of TLR4/MyD88-dependent signaling to hepatic inflammation. While TLR4 has not been functionally verified as a direct molecular target of CA, the consistent inhibitory effect of CA on this signaling axis across diverse species and inflammatory models strongly indicates that the TLR4-dependent cascade acts as a key node mediating the anti-inflammatory actions of CA.

TAK1 is a critical regulatory node downstream of TLR4 and serves as a molecular hub linking TLR4 to downstream kinase cascades (Wang et al., 2021). We incorporated TAK1 into molecular docking, which predicted favorable interactions between CA and TAK1, suggesting CA may interact with TAK1 to modulate downstream signaling. In vivo, LPS upregulated TAK1 mRNA in broiler liver, and CA reversed this increase (Moon and Ro, 2021; Zulfiqar et al., 2025). Existing literature shows JNK and p38 are core mediators of hepatic inflammatory injury, and p38 plays a dominant role in stress-induced hepatocyte apoptosis (Westenberger et al., 2021). Notably, stable phosphorylated JNK bands could not be obtained in repeated LMH cell assays in our work; thus only JNK transcriptional changes were evaluated here, while phosphorylation of TAK1 and p38 was detected in vitro.

In the present study, we integrated bioinformatic analysis, molecular docking, an in vivo broiler model and in vitro LMH cell experiments to explore the protective effects of CA against LPS-induced hepatic inflammatory injury. Notably, bioinformatic analysis and molecular docking serve only as in-silico predictive tools and cannot confirm actual physical interactions between CA and target proteins. CA appears to modulate the TLR4/MyD88/TAK1/MAPK signaling cascade, partially through down-regulating transcription of upstream receptor and adaptor genes in vivo and suppressing TAK1 and p38 phosphorylation in LMH cells in vitro. Altered activity of this core inflammatory signaling axis is accompanied by reduced pro-inflammatory cytokine secretion and improved hepatic pathological manifestations. Taken together, our multi-level evidence spanning in silico prediction to wet-lab experiments suggest that CA exerts hepatoprotective and anti-inflammatory activities in LPS-challenged broilers.

This study has several limitations. First, we are unable to distinguish whether the observed effects arise from direct binding of CA to target proteins or indirect cellular feedback responses. Second, although we detected altered TAK1 and p38 phosphorylation in LMH cells, phosphorylated forms of these proteins were not validated via Western blot in broiler liver tissues. Third, histopathological assessment relied solely on representative H&E micrographs, without blinded semi-quantitative scoring. Further functional studies, including gene knockdown and pathway-specific inhibitor assays, are required to clarify the precise regulatory pattern of CA-modulated phosphorylation and identify its direct molecular targets within this signaling axis. Fourth, the reduced transcript abundance of inflammatory cytokines and signaling kinases following CA treatment could partly stem from general cytoprotective effects instead of specific modulation of the TLR4/MAPK inflammatory signaling cascade. Additional measurements such as LDH release, cell-normalized cytokine quantification and standardized apoptosis assays would be required to clearly discriminate cytoprotection from direct pathway regulation, and these assays were not included in the present

experimental design.

In summary, the hepatoprotective effect of CA against LPS-provoked hepatic inflammation is associated with modulation of the TLR4/MAPK signaling pathway. This work expands our understanding of chicoric acid as a natural bioactive compound and provides experimental support for its potential application as a feed additive for mitigating inflammatory liver disorders in poultry.

Conclusion

Molecular docking suggested potential interactions between CA and p38. In broilers, CA downregulated LPS-induced hepatic mRNA expression of TAK1, JNK and p38. Using LMH cells, we further verified that CA inhibited the phosphorylation of TAK1 and p38, while the total protein levels of these targets remained unchanged. Collectively, CA exerts anti-inflammatory and hepatoprotective functions against LPS-elicited liver injury, and these correlative findings indicate that this protective effect is at least partially attributed to the suppression of the TLR4/TAK1–p38 signaling cascade.

Author contribution

Qingqing Han conceived the overall study framework, performed the experiments, analyzed and interpreted the data, drafted the manuscript, approved the final version, and is accountable for all aspects of this work. **Leying Ma** collected and analyzed experimental data, drafted the manuscript, critically revised the manuscript for important intellectual content, approved the final version, and is accountable for all aspects of this work. **Zhanfan He** contributed to the conception of the study, critically revised the manuscript for important intellectual content, approved the final version, and is accountable for all aspects of this work. **Zhou Shuai** performed histopathological observation and biochemical indicator measurements, interpreted part of the data, critically revised the manuscript for important intellectual content, approved the final version, and is accountable for all aspects of this work. **Gengnan Wang** designed the experimental protocols, supervised the research, critically revised the manuscript for important intellectual content, approved the final version, and is accountable for all aspects of this work. All authors confirm that they meet all four authorship criteria specified by the journal.

Disclosures

All authors of this manuscript agree to submit it to your journal for review. This declaration explicitly states that the manuscript remains unpublished and unreviewed by any other scholarly publication and will not be submitted to any other journals until a formal decision is rendered by this journal.

Acknowledgments

This work was supported by the National Natural Science Foundation of China (32002343), the Hebei Natural Science Foundation (C2022204090), and the Veterinary Biological Technology Innovation Center of Hebei Province.

References

Chen, J., Wang, H., Wu, Z., Gu, H., Li, C., Wang, S., Liu, G., 2022. Effects of 5-aminolevulinic acid on the inflammatory responses and antioxidative capacity in broiler chickens challenged with lipopolysaccharide. Animal. 16, 100575. CrossRef.

Chen, J., Yang, W., Liu, H., Niu, J., Liu, Y., Cheng, Q., 2024. Protective effect of Macleaya cordata isoquinoline alkaloids on lipopolysaccharide-induced liver injury in broilers. Anim. Biosci. 37, 131–141. CrossRef.

Chen, Y., Liu, Y., Zhao, C., Ma, J., Guo, J., 2025. Antibiotic resistance gene pollution in poultry farming environments and approaches for mitigation: a system review. Poult. Sci. 104, 104858. CrossRef.

Cheng, G.M., Cheng, H., 2024. Overcoming China's animal waste disposal challenge brought by elevated levels of veterinary antimicrobial residues and antimicrobial resistance. Environ. Int. 191, 109009. CrossRef.

Ding, H., Ci, X., Cheng, H., Yu, Q., Li, D., 2019. Chicoric acid alleviates lipopolysaccharide-induced acute lung injury in mice through anti-inflammatory and anti-oxidant activities. Int. Immunopharmacol. 66, 169–176. CrossRef.

Guo, H., Liu, S., You, M., Zhang, X., Wu, S., Zhao, X., Shi, W., Ma, N., 2026. Total flavonoids from Abrus cantoniensis alleviate fatty liver hemorrhagic syndrome in laying hens by regulating inflammation, oxidative stress, and cecal metabolites and microbiota. Anim. Nutr. 25, 144–159. CrossRef.

Huang, Y., Zong, S., Xu, D., He, J., Zhang, Y., Qian, M., Li, Y., Guo, B., Han, J., Qu, D., 2025. Metagenomic analysis reveals differences in antibiotic resistance and transmission risks across various poultry farming models. Sci. Total Environ. 980, 179519. CrossRef.

Huynh, D.T.N., Baek, N., Sim, S., Myung, C., Heo, K., 2020. Minor ginsenoside Rg2 and Rh1 attenuates LPS-induced acute liver and kidney damages via downregulating activation of TLR4-STAT1 and inflammatory cytokine production in macrophages. Int. J. Mol. Sci. 21, 6656. CrossRef.

Ivanova, S., Sukhikh, S., Popov, A., Shishko, O., Nikonov, I., Kapitonova, E., Krol, O., Larina, V., Noskova, S., Babich, O., 2024. Medicinal plants: a source of phytobiotics for the feed additives. J. Agric. Food Res. 16, 101172. CrossRef.

Korver, D.R., 2023. Review: current challenges in poultry nutrition, health, and welfare. Animal 17, 100755. CrossRef.

Li, M., Zhao, H., Wu, J., Wang, L., Wang, J., Lv, K., Liu, S., Wang, M., Guan, W., Liu, J., Ho, C.T., Li, S., 2020. Nobiletin protects against acute liver injury via targeting c-Jun N-Terminal Kinase (JNK)-induced apoptosis of hepatocytes. J. Agric. Food Chem. 68, 7112–7120. CrossRef.

Liao, C.H., Lin, J.Y., 2011. Lotus (Nelumbo nucifera Gaertn) plumule polysaccharide protects the spleen and liver from spontaneous inflammation in non-obese diabetic mice by modulating pro-/anti-inflammatory cytokine gene expression. Food Chem. 129, 245–252. CrossRef.

Liu, J., Kang, R., Tang, D.L., 2024. Lipopolysaccharide delivery systems in innate immunity. Trend. Immunol. 45, 274–287. CrossRef.

Mei, W., Hao, Y., Xie, H., Ni, Y., Zhao, R., 2020. Hepatic inflammatory response to exogenous LPS challenge is exacerbated in broilers with fatty liver disease. Animals (Basel), 10030514.

Moon, H., Ro, S.W., 2021. MAPK/ERK signaling pathway in hepatocellular carcinoma. Cancers (Basel), 13123026.

Peng, Y., Sun, Q.C., Park, Y., 2019. The bioactive effects of Chicoric acid As a functional food ingredient. J. Med. Food 22, 645–652. CrossRef.

Wan, S.S., Li, X.Y., Liu, S.R., Tang, S., 2024. The function of carnosic acid in lipopolysaccharides-induced hepatic and intestinal inflammation in poultry. Poult. Sci. 103, 103415. CrossRef.

Wang, D., Gao, Q., Zhao, G., Kan, Z., Wang, X., Wang, H., Huang, J., Wang, T., Qian, F., Ho, C.T., Wang, Y., 2018. Protective effect and mechanism of theanine on lipopolysaccharide-induced inflammation and acute liver injury in mice. J. Agric. Food Chem. 66, 7674–7683. CrossRef.

Wang, L., Zhang, X., Lin, Z.B., Yang, P.J., Xu, H., Duan, J.L., Ruan, B., Song, P., Liu, J.J., Yue, Z.S., Fang, Z.Q., Hu, H., Liu, Z., Huang, X.L., Yang, L., Tian, S., Tao, K.S., Han, H., Dou, K.F., 2021. Tripartite motif 16 ameliorates nonalcoholic steatohepatitis by promoting the degradation of phospho-TAK1. Cell Metab. 33, 1372–1388.e7. CrossRef.

Wang, L.J., Cheng, J., Shan, X.M., Shi, Y.N., Wang, Q.F., Pan, S.F., Lu, Y., 2026. Sodium butyrate ameliorates lipid metabolism disorder, intestinal injury, and microbial dysbiosis in broilers under lipopolysaccharide-induced immune stress condition. Poult. Sci. 105, 106263. CrossRef.

Wang, N., Feng, B.N., Hu, B., Cheng, Y.L., Guo, Y.H., Qian, H., 2022. Neuroprotection of chicoric acid in a mouse model of Parkinson's disease involves gut microbiota and TLR4 signaling pathway. Food Funct. 13, 2019–2032. CrossRef.

Wang, Q., Niu, J., Liu, Y., Jiao, N., Huang, L., Jiang, S., Yan, L., Yang, W., Li, Y., 2022. Supplementation of paraformic acid as a substitute for antibiotics in the diet improves growth performance and liver health in broiler chickens. Animals (Basel) 12, 2825. CrossRef.

Westenberger, G., Sellers, J., Fernando, S., Junkins, S., Han, S.M., Min, K., Lawan, A., 2021. Function of mitogen-activated protein kinases in hepatic inflammation. J. Cell Signal. 2, 172–180.

Wu, D., Cui, D., Zhou, M., Ying, Y., 2022. Information perception in modern poultry farming: a review. Comput. Electron. Agric. 199, 107131. CrossRef.

Xiao, H., Xie, G., Wang, J., Hou, X., Wang, X., Wu, W., Liu, X., 2013. Chicoric acid prevents obesity by attenuating hepatic steatosis, inflammation and oxidative stress in high-fat diet-fed mice. Food Res. Int. 54, 345–353. CrossRef.

Xing, X., Hu, H., Hu, H., Chu, J., Li, S., Han, D., Zhao, B., Li, S., 2026. Quercetin from Penthorum chinense Pursh protects against LPS-induced liver inflammation in chickens via suppressing pyroptosis-macrophage polarization crosstalk. J. Ethnopharmacol. 355, 120665. CrossRef.

Xing, Y., Zheng, Y., Yang, S., Zhang, L., Guo, S., Shi, L., Xu, Y., Jin, X., Yan, S., Shi, B., 2023. Artemisia ordosica polysaccharide ameliorated LPS-induced growth inhibition and intestinal injury in broilers through enhancing immune-regulation and antioxidant capacity. J. Nutr. Biochem. 115, 109284. CrossRef.

Xu, Q., Xu, J., Zhang, K., Zhong, M., Cao, H., Wei, R., Jin, L., Gao, Y., 2021. Study on the protective effect and mechanism of Dicliptera chinensis (L.) Juss (Acanthaceae) polysaccharide on immune liver injury induced by LPS. Biomed. Pharmacother. 134, 111159. CrossRef.

Yang, M., Wu, C., Zhang, T., Shi, L., Li, J., Liang, H., Lv, X., Jing, F., Qin, L., Zhao, T., Wang, C., Liu, G., Feng, S., Li, F., 2022. Chicoric Acid: natural occurrence, chemical synthesis, biosynthesis, and their bioactive effects. Front. Chem. 10, 3389.

Yu, J., Fu, R., Buhe, A., Xu, B., 2024. Quercetin attenuates lipopolysaccharide-induced hepatic inflammation by modulating autophagy and necroptosis. Poult. Sci. 103, 103719. CrossRef.

Zhang, B., Hong, L., Ke, J., Zhong, Y., Cao, N., Li, W., Xu, D., Tian, Y., Huang, Y., Chen, W., Li, B., 2023. Polysaccharide of Atractylodes macrocephala Koidz alleviate lipopolysaccharide-induced liver injury in goslings via the p53 and FOXO pathways. Poult. Sci. 102, 102480. CrossRef.

Zhang, J., Zhang, Y., Wang, Y., Hou, W., Liu, D., Miao, Z., 2024. Research note: Poria cocos polysaccharide alleviates lipopolysaccharide-induced intestinal inflammation and barrier damage in broiler chickens. Poult. Sci. 103, 104126. CrossRef.

Zhang, X., Sun, L., Wu, M., Yu, C., Zhao, D., Wang, L., Zhang, Z., Yi, D., Hou, Y., Wu, T., 2024. Effect of supplementation with Lactobacillus rhamnosus GG powder on intestinal and liver damage in broiler chickens challenged by lipopolysaccharide. Front. Microbiol. 15, 1466274. CrossRef.

Zheng, B., Jiang, C., Wang, Z., Zhang, Q., Du, H., Huang, N., Wang, J., Du, J., Zhang, D., Sun, R., Wang, D., 2026. An arabinogalactan from Bupleurum chinense DC. attenuates LPS-induced inflammation in RAW264.7 macrophages. Carbohydr. Polym. 380, 125053. CrossRef.

Zulfiqar, Z., Asif, M.A., Al-Mitib, L., Alharbi, K., Hossain, T., Yao, H., Zhu, X., Wang, Z., Sun, H., Cui, Y., Liu, B., Shi, Y., 2025. Zn glycine mitigates the LPS-induced hepatic injury and inflammation through NrF2/NFκB signaling in geese. Poult. Sci. 104, 105772. CrossRef.